Astro. Lett. and Communications, 1995, Vol. 32, pp. 95–103
Reprints available directly from the publisher
Photocopying permitted by license only

Analysis of Topology of the COBE-DMR First Year Maps[1]

S. TORRES *International Centre for Relativistic Astrophysics, Dip. Fisica, Università di Roma, Pzle. Aldo Moro, 2, 00185, Rome, Italy, and Centro Internacional de Física, and Universidad de los Andes, Bogotá, Colombia*

(Received 3 January 1994; in final from 7 April 1994)

An algorithm to identify hot/cold spots in anisotropy maps was used to compute the genus and number of spots descriptors in the first year COBE-DMR sky maps. By means of Monte Carlo simulations it is shown that the structure present in these maps is consistent with a scale invariant primordial spectrum. An unbias estimation of the coherence angle of the fluctuation field, based on the genus curve, gives a spectral index $n = 1.2 \pm 0.3$

1. INTRODUCTION

Information about the spectrum of primordial matter density fluctuations, $P(k)$, can be inferred from the autocorrelation function (acf) of the cosmic microwave background (CMB) temperature. An alternative way to test hypotheses for models of $P(k)$ is to look at the statistics of the geometric properties of anisotropy spots on CMB maps. The most important advantages of this second approach are that, unlike acf computations, topological analysis does not assume an ergodic radiation field (Cayón *et al.*, 1991; Vittorio and Scaramella, 1991), and it provides information about $P(k)$ independent of its normalization. In addition to using the analysis of geometric properties of anisotropy spots to test hypotheses, this analysis technique can be used as a diagnostic tool to detect the presence of a non random component on CMB maps, such as foreground signals; as an unbias estimator of the coherence angle of the underlying random field (Adler, 1981); and to verify the Gaussianity of primordial fluctuations, thus providing a test for models of structure formation that rely on primordial seeds, such as cosmic strings (Bennett *et al.*, 1992) or texture (Park *et al.*, 1991).

The excursion set of a random field is defined as the domain of all the points where the field takes values $T \geq T_\nu = \nu\sigma$, where σ and ν denote the standard deviation and threshold level respectively.

There are several topological descriptors that have been studied and used to characterize the properties of the excursion regions on CMB maps (Sazhin, 1985; Vittorio and Juszkiewics, 1987; Bond and Efstathiou, 1987; Coles and Barrow, 1987; Coles, 1988a; Coles, 1988b; Gott *et al.*, 1990; Martínez–González, 1989): the number of spots N_ν on the sphere with temperature above T_ν, and below $-T_\nu$; their mean area,

A_ν; the total curvature of their boundary, or genus G_ν; the length of contour levels, L_ν; the total excursion area of hot spots, a_ν; the number of up crossings for the one dimensional case and the Euler–Poincaré characteristic which is the generalization of the number of up-crossings for the two dimensional case (Adler, 1981).

From the theory of the geometric properties of excursion sets it is possible to derive analytical expressions for some of the above mentioned descriptors. In particular, for two dimensional, stationary, isotropic, Gaussian random fields these geometric properties depend only on the coherence angle parameter: $\theta_c^2 = -C(0)/C''(0)$. The mean number of spots and genus on the 4π surface, and the total area of the excursion set are:

$$\langle N_\nu \rangle = \frac{2}{\pi\theta_c^2} \frac{\exp(-\nu^2)}{\operatorname{erfc}(\nu/\sqrt{2})} \tag{1}$$

$$\langle G_\nu \rangle = \left(\frac{2}{\pi}\right)^{1/2} \frac{\nu}{\theta_c^2} \exp\left(-\frac{\nu^2}{2}\right) \tag{2}$$

$$\langle a_\nu \rangle = 2\pi \operatorname{erfc}(\nu/\sqrt{2}), \tag{3}$$

notice that the total area of the excursion set is independent of the parameter θ_c. This fact will be used to identify the presence of possible systematic effects in the data.

The topology of the first year COBE-DMR maps was analyzed in order to check the consistency of the Harrison–Zeldovich power spectrum, $P(k) \propto k$ (Harrison, 1970; Zeldovich, 1972), with the data. The COBE-DMR results are described by Smoot *et al.* (1992) and references therein.

ALGORITHMS TO COMPUTE TOPOLOGICAL DESCRIPTIONS

COBE data is pixelized by means of a projection of the 2D celestial sphere onto a cube (the skycube), where the sphere is circumscribed (Torres *et al.*, 1989). Each side of the cube is divided into 1024 pixels for a total of 6144 pixels, each one with angular dimensions $\approx 2.6^\circ \times 2.6^\circ$, comparable to COBE's angular resolution. Pixel numbering is done by packing in a single word the face number and the Cartesian coordinates of the pixels on that face. Having the address of a pixel stored in the pixel number is a convenience that has been exploited to develop efficient algorithms.

The advantages offered by this pixelization scheme on the skycube and the desire to work with the data as close to its original form as possible, made the skycube an obvious choice as a data-base structure for the hot spots algorithms used here. An added advantage of the skycube is that it is a flat surface, thus avoiding the problems of evaluating the topological descriptors in the presence of poles.

Since the objects that, are being studied (hot spots) are defined in terms of a threshold level ν, the first step of the analysis is to produce a binary map for each threshold level. A binary map consists of 1's and 0's according to its corresponding pixel having a temperature greater than or equal to T_ν, or less than T_ν respectively.

The HOTS program: Hot spots are then found on a bitmap by forming tree data structures. The skycube is traversed, as soon as a lit pixel is found it becomes the root node and all the neighbor pixels that are lit become children nodes of the same tree. A tree is completed when no more hot pixel neighbors are found. The number of hot spots in the map at this threshold equals the number of trees found. The area of the hot spot is the total number of nodes in the tree. Other geometric characteristics can easily be computed by using the tree data structure. Length of contour levels are found by counting for each node pixel the number of sides whose neighbor pixel is not lit.

An estimate of the eccentricity of hot spots can be found by first finding the coordinates of the center of the hot spot, and then evaluating the distance of all pixels to the center. The eccentricity is the ratio of the smallest to the largest distance. Finding the center of a hot spot can be done considering that it is a uniform sheet of mass. The center is then given by coordinates of the center of mass. The algorithm given by Adler (1981) to evaluate the Euler–Poincaré characteristic can be easily implemented using tree data structures.

The total curvature index, or genus of a map at a threshold level is the total number of hot spots minus the number of holes in them (Gott *et al.*, 1992). The number of holes at a given threshold level is found using the hot spot algorithm recursively with an input binary map formed by negating the binary sky map at the same threshold.

In order to test the algorithm, simulated maps of a Gaussian random field were generated as described below and their genus and hot spot number density, areas and contour lengths were evaluated by HOTS. Figure 1a shows the simulated total area mean values with theoretical a_ν while Figure 1b does the same for the genus. The agreement is good.

When an equatorial band is excluded from the maps, in order to remove the contribution of the galaxy, a boundary is introduced and as a consequence there appear deviations of the G_ν and N_ν curves with respect to their theoretical values. To take into account this effect, all Monte Carlo generated data sets contain identical treatment, including galactic cuts, as done in the analysis of the experimental data.

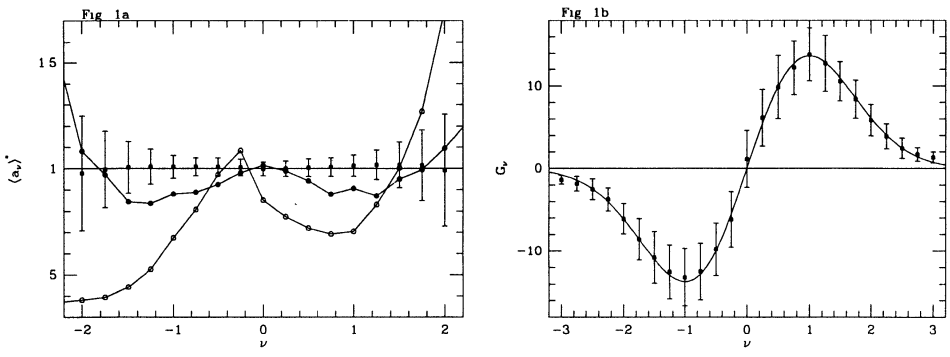

FIGURE 1 a) Mean value of the total area of excursion divided by $2\pi\,\mathrm{erfc}(\nu/\sqrt{2})$ at different threshold levels. The horizontal line corresponds to the expected theoretical value for a random field, independent of its coherence angle. Open squares with 1 sigma error bars are for Monte Carlo data. Circles are for the $31(A+B)$ DMR maps with a 30° (filled in circles) and a 10° (open circles) galactic cut. b) Mean values of the genus as a function of threshold for Monte Carlo simulations of a Gaussian random field. The solid curve is the theoretical function.

MONTE CARLO SIMULATIONS

A CMB map as observed by COBE can be simulated by assigning to each pixel i a temperature given by the real part of:

$$T_i = T_0\left(1 + \sum_{l=2}\sum_{m=-l}^{l} a_{lm} W_l Y_{lm}(\theta_i, \phi_i)\right), \tag{4}$$

with T_0 the monopole temperature of 2.735 K (Mather *et al.*, 1990), and θ_i, ϕ_i the zenith and azimuth angles of a unit vector to pixel i. The dipole term ($l = 1$), which is excluded, is dominated by the Doppler effect due to our present peculiar velocity relative to the co-moving frame. The finite beamwidth, σ_b, of the instrument enters in the term W_l as a high-pass filter (Scaramella & Vittorio, 1988): $W_l = \exp[-0.5\sigma_b^2 l(l+1)]$. For random Gaussian fields and harmonic coefficients are random variables with zero mean, and follow a Gaussian probability distribution. Their variance is determined by the spectrum of primordial matter density perturbations.

Since DMR's beam size ($> 2°$) is probing scales beyond which only fluctuations of the gravitational potential on the surface of last scattering affect the isotropy of the CMB, the Sachs–Wolfe effect alone suffices for the determination of the variances (Sachs & Wolfe 1967). For power law spectra, $P(k) \propto k^n$, the Bond–Efstathiou formula (1987) for the variances is adequate since only the contribution of terms up to $l \sim 30$ is important after beamwidth filtering and further Gaussian smoothing are done on the maps. Instrumental noise and sky coverage is taken into account by adding to each pixel a noise term equals to a Gaussian random number with dispersion equals to the one-observation measurement noise, T_{noise}, divided by $\sqrt{N_{\text{obs.}}}$ The number of observations N_{obs} is included in the original skymaps. The slope of a plot of T^2 versus $1/N_{\text{obs}}$ with properly binned data is used to find T_{noise}. The noise levels found with this procedure for each channel at each one of the three DMR frequencies was found to be within 7% of the nominal value.

For the Monte Carlo generation of maps, two maps (A and B) were generated separately, each with its corresponding noise level, then added and subtracted to form the $(A + B)$ and $(A - B)$ maps. Finally, 2.9° Gaussian smoothig was applied to the maps.

Each sky map produced is one realization of the ensemble. To each realization, HOTS was used to extract G_ν, N_ν, A_ν and L_ν. After 400 realizations were done, their respective mean value and dispersion were computed.

Figures 2a–2d show the mean values and their 1 sigma error bars for the number of spots and genus. In these plots it is shown what would be seen by the 53 GHz DMR radiometers observing a universe with Harrison–Zeldovich primordial fluctuations. In the same plot it is also shown the values of topological descriptors as obtained from maps made with pure instrumental noise. The separation between these two curves is an indication of both the power of a statistical test and the efficiency of a topological descriptor as discriminator. Noisier maps for example would result in "noise" and "signal" curves which are too close. The L_ν and A_ν curves (not shown) for noise and signal are too close to each other, rendering these descriptors inefficient for testing power spectra with index close to one. Genus and number of spots will be the only descriptors used here to test that hypothesis.

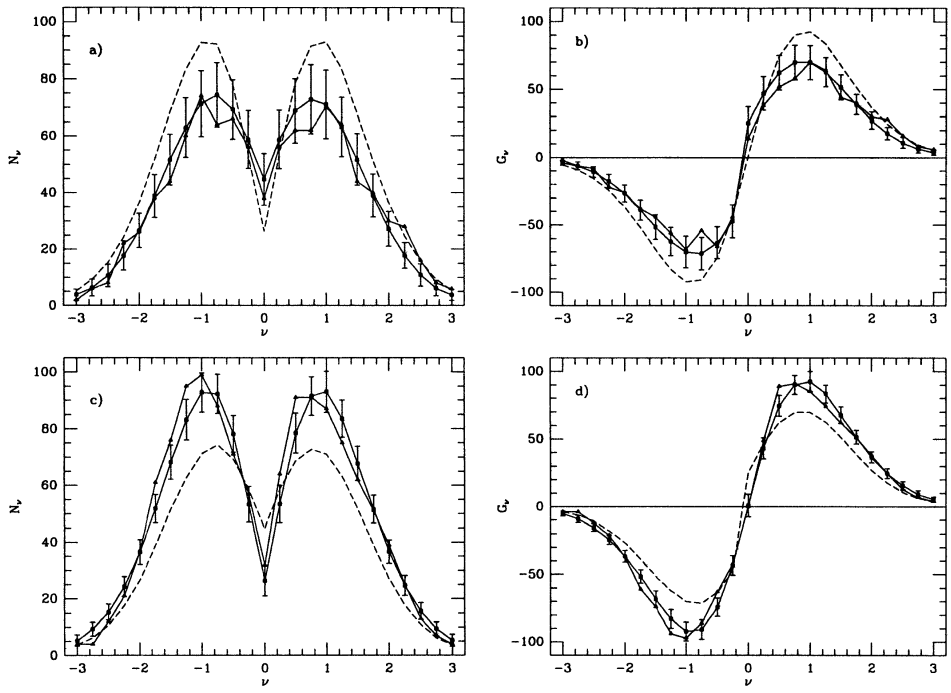

FIGURE 2 a) Number of spots normalized to the area of the sphere for the COBE-DMR 53($A + B$) data (triangles) and Monte Carlo simulations for the COBE 53 GHz radiometers observing a Universe with a Harrison–Zeldovich spectrum (solid line with error bars) and with instrumental noise only (short dashed line). b) same as a) for genus. c) and d) are the same as a) and b) but the data (triangles) show the COBE-DMR 53 GHz ($A - B$) maps and the short dashed curve corresponds to the Harrison–Zeldovich simulations.

To compare a cosmological model with the data, the χ^2 and the cumulative probability distribution of χ^2 are constructed from the Monte Carlo data as suggested by Gott *et al.* (1992). That is, for each Monte Carlo map the values of a topological descriptor U_ν at 25 threshold levels ν: $-3.0 \ldots 3.0$ are used to compute the normalized χ^2:

$$\chi^2 = \frac{1}{24} \sum_{j=1}^{25} \frac{(U_j - \langle U_j \rangle)^2}{\sigma_j^2}, \tag{5}$$

where $\langle U_j \rangle$ and σ_j are calculated from the set of Monte Carlo simulations for a particular cosmological model.

PREPARATION OF DATA

Four of the six original COBE-DMR sky maps were used: 53A and B and 90A and B. The data comes in the skycube format discussed above, in Geocentric Ecliptic coordinates. Before the analysis of peak statistics can be performed it is necessary to remove the Doppler component consisting primarily of the dipole anisotropy but including a 1.2 μK kinematic quadrupole term, and to rotate the maps to galactic equatorial coordinates. To reduce the noise on the maps, an additional Gaussian smoothing of 2.9° was done.

To check for the integrity of the data and the analysis software I have computed and compared with COBE's published results (Smoot *et al.*, 1992), the following quantities: the dipole, the rms sky variation on a 10° scale, and the quadrupole. The dipole and quadrupole was obtained with a least squares fit of the map to the harmonic expansion (4). The dipole amplitude and orientation are in agreement with Smoot *et al.* (1992): $\Delta T/T = 3.36 \pm 0.04$, $l = 264° \pm 1°$, $b = 48° \pm 1°$. These numbers are weighted averages with 31B excluded. COBE's error bars for the dipole are larger because here I have not considered systematic effects, only statistical errors are quoted.

To compare the quadrupole numbers against COBE's results I have used the rms value Q_{rms} and the direction of the axis of symmetry connecting the two minimum points of the quadrupole. The principal axes are found making an analogy with the mechanics of rigid bodies. If one builds a unit radius shell with a surface mass distribution given by the $l = 2$ term in the harmonic expansion (4):

$$\rho = \sum q_i Q_i, \tag{6}$$

with

$$Q_1 = \frac{\varepsilon}{2}(3\cos^2\theta - 1), \tag{7}$$

$$Q_2 = \sqrt{3}\varepsilon \sin\theta \cos\theta \cos\phi, \tag{8}$$

$$Q_3 = \sqrt{3}\varepsilon \sin\theta \cos\theta \sin\phi, \tag{9}$$

$$Q_4 = \frac{\sqrt{3}\varepsilon}{2} \sin^2\theta \cos 2\phi, \tag{10}$$

$$Q_5 = \frac{\sqrt{3}\varepsilon}{2} \sin^2\theta \sin 2\phi, \tag{11}$$

$\varepsilon^2 = 5/4\pi$, then the eigenvectors of the moment of inertia matrix are the sought axes of symmetry. The matrix in terms of the quadrupole coefficients is:

$$I_{ij} = \begin{bmatrix} \frac{q_1}{3\varepsilon} - \frac{q_4}{\sqrt{3}\varepsilon} & -\frac{q_5}{\sqrt{3}\varepsilon} & \frac{q_2}{\sqrt{3}\varepsilon} \\ I_{12} & \frac{q_4}{\sqrt{3}\varepsilon} + \frac{q_1}{3\varepsilon} & \frac{q_3}{\sqrt{3}\varepsilon} \\ I_{13} & I_{21} & -\frac{2q_1}{3\varepsilon} \end{bmatrix} \tag{12}$$

It is found that the use of the principal axes of the quadrupole are not only useful to visualize the quadrupole orientation, but also in this case it reveals a possible correlation between the quadrupole and the galaxy, as can be seen by the increasing alignment of the quadrupole with the galaxy as the galactic cut is reduced (Figure 3). Notice that the quadrupole orientation goes to its convergence value much faster for those maps less contaminated with galactic emission, as expected.

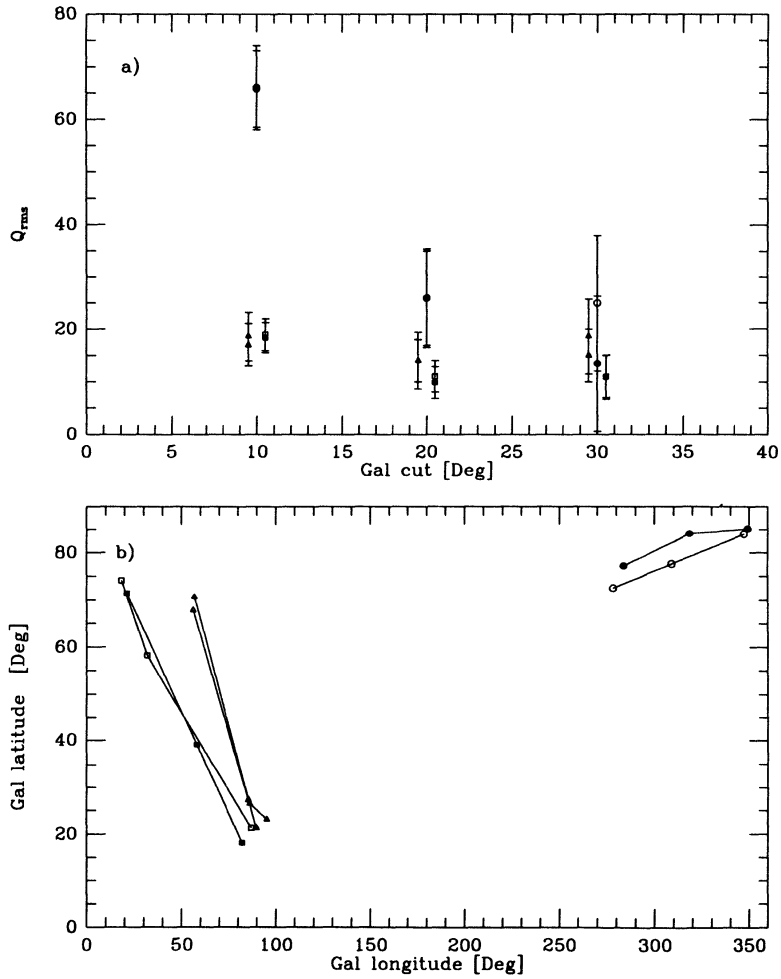

FIGURE 3 a) Quadrupole *rms* as obtained here (filled in polygons) and by Smoot *et al.* (1992) (open polygons) for different galactic cuts, 31 GHz (circles), 53 GHz (squares) and 90 GHz (triangles). b) Orientation of the principal axis of the Quadrupole on the *l*, *b* plane for different cuts of the equatorial band. Filled in polygons are data points obtained in this analysis, open polygons are from Smoot *et al.* (1992). The data corresponds to three galactic cuts $|b| > 10°, 20°$, and $30°$, the smaller $|b|$ values are more strongly aligned with the galaxy.

ANALYSIS AND CONCLUSIONS

The total area of the excursion set (3) is a good topological descriptor to detect the presence of a non-random component in CMB maps. Figure 1a is a plot of a_ν versus ν and illustrates what would be obtained for a pure random field independent of its coherence angle. Curves of a versus threshold for the 31 GHz DMR $(A + B)$ map in the same figure show large deviations. These deviations become more pronounced when the galactic cut is smaller, indicating that the galactic contamination at high latitudes is the most likely source responsible for the observed effect. For the 53 and 90 $(A + B)$ maps no deviations beyond the 1 sigma area in Figure 1a were seen for galactic cuts $|b| > 25$ degrees.

Genus and number of spot descriptors were used to test for the consistency of a Harrison–Zeldovich spectrum of primordial perturbations. It is found that the null hypothesis (i.e. the structure on COBE maps is due to instrumental noise alone) can be rejected with a very high confidence level (see Figure 2): the χ^2 obtained for the COBE-DMR data when the null hypothesis is assumed in the Monte Carlo procedure are very high: 6.75 and 7.51 for the number of spots and genus for the 53 GHz channels, 3.59 and 4.38 respectively for the 90 GHz channels. The corresponding probabilities of obtaining such a high χ^2 are $< 1/400$ for all these cases. It is clear that there is structure on the DMR maps from astrophysical or cosmological origin. A detailed analysis of possible noncosmological sources (Bennett *et al.*, 1993) shows that the contribution to the DMR maps of known point sources in infrared, radio and x-ray catalogues is negligible. Ruling out foreground sources the most probable cause of the structure seen is from cosmological origin.

Using the topological descriptors genus and number of spots computed on Monte Carlo realizations of CMB maps with a Harrison–Zeldovich (normalized to 16 μK Q_{rms-PS}) power spectrum it is found that this model is consistent with DMR data with a high confidence level (Figure 2) in agreement with a preliminary hot spot analysis (Gurzadyan and Torres 1993). The χ^2 of COBE-DMR data when the Harrison–Zeldovich hypothesis is assumed in the Monte Carlo procedure are very low: 0.62 and 1.48 for the 53 and 90 GHz number of spots, and 0.72 and 1.73 for the 53 and 90 GHz genus. The corresponding probabilities for such a low χ^2 values are 95% and 14% for the 53 and 90 GHz number of spots and 83% and 8% for the 53 and 90 GHz genus. Other values for the spectral index n are also consistent with the data. To see the dependence of the genus and number of spots on the spectral index, several sets of

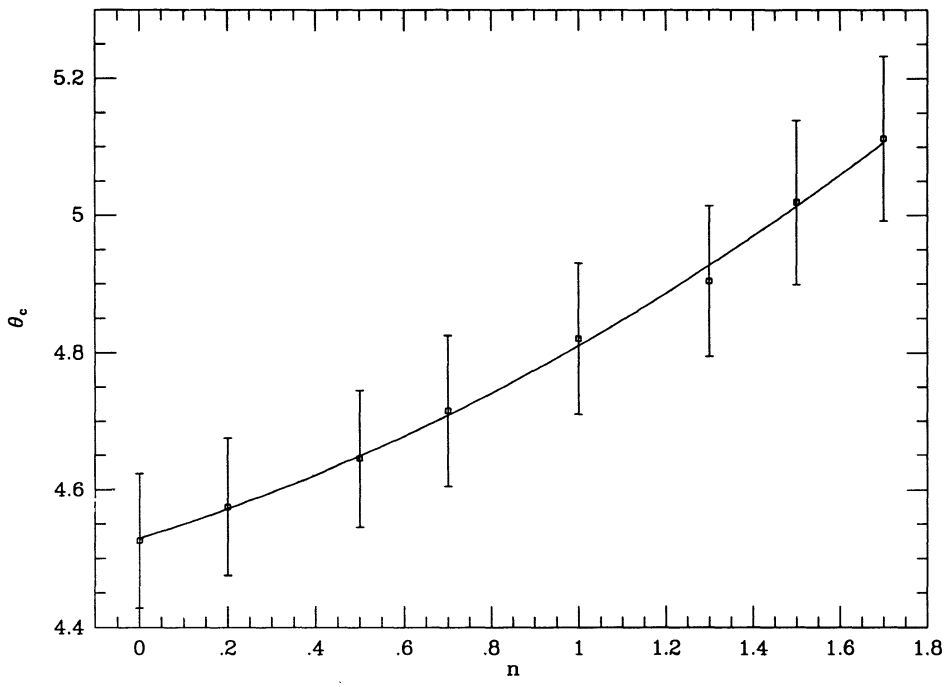

FIGURE 4 Coherence angle in degrees versus spectral index as obtained from the Monte Carlo runs.

Monte Carlo realizations were generated with fixed Q_{rms-PS} normalization and variable n. For each spectral index, the genus curve as a function of threshold ν was fitted using (2) in order to obtain the best θ_c that fits the data. The dependence of the coherence angle with spectral index is alomost linear, as can be seen in Figure 4. With the error bars for θ_c obtained from the Monte Carlo simulations it is now possible to estimate the best n with its error bars by fitting the genus curves of COBE's maps to get their coherence angle. Based on the the genus curves, the coherence angle for the 53 GHz $(A + B)$ DMR map is $\theta_c = 4.9^\circ \pm 0.1^\circ$ which gives a spectral index $n = 1.2 \pm 0.3$ in agreement with the values obtained by Smooth *et al.* (1992) based on the fit to the acf.

ACKNOWLEDGEMENTS

I thank Prof. Remo Ruffini, Roberto Fabbri and George Smoot for their useful comments. This research has been supported by Colciencias of Colombia project # 1204-05-007-90 and the European Community under contract No. CI1-CT92-0013. The support of the Super Computer Computations Research Institute of Florida State University, where some of the Monte Carlos were done, is greatly appreciated. The COBE datasets were developed by the NASA Goddard Space Flight Center under the guidance of the COBE Science Working Group and were provided by the NSSDC.

REFERENCES

Adler, R. J., 1981, The geometry of Random Fields (New York: Wiley).
Gott, J. R., *et al.*, 1990, *Ap. J.*, **352**, 1.
Gurzadyan, V., and Torres, S., 1993, in *Present and Future of the Cosmic Microwave Background*, Edts. Sanz, J. L., Martínez–González and E. Cayón, L., Springer-Verlag, **429**, 139.
Bennett, C. *et al.*, 1993, *Ap. J.*, **414**, L77.
Bennett, D. P., Stebbins, A., and Bouchet, F. R., 1992, *Ap. J.*, **399**, L5.
Bond, J. R. and Efstathiou, G., 1987, *MNRAS*, **226**, 655.
Cayón, L., Martínez–González, E., and Sanz, J. L. 1991, *MNRAS*, **253**, 599.
Coles, P., 1988a, *MNRAS*, **231**, 125.
Coles, P. 1988b, *MNRAS*, **234**, 509.
Coles, P., and Barrow, D., 1987, *MNRAS*, **228**, 407.
Harrison, E. R., 1970, *Phys. Rev. D*, **1**, 2726.
Martíez–González, E., and Sanz, J. L., 1989, *MNRAS*, **237**, 939.
Mather, J. C. *et al.*, 1990, *Ap. J.*, **354**, L37.
Park, C., Spergel, D. N., and Turok, N., 1991, *Ap. J.*, **372**, L53.
Sachs, K., and Wolfe, A. M., 1967, *Ap. J.*, **147**, 73.
Sazhin, M. V., 1985, *MNRAS*, **216**, 25p.
Scaramella, R., and Vittorio, N., 1988, *Ap. J.*, **331**, L53.
Smoot, G. F. *et al.*, 1992, *Ap. J.*, **396**, L1.
Torres, S., *et al.*, 1989, in *Data Analysis in Astronomy*, ed. V. di Gesu, L. Scarsi and M. C. Maccarone (Erice, 1988), **40**, 319–333.
Vittorio, N., and Scaramella, R., 1991 in *Physical Cosmology*, Edts. Blanchard, A. *et al.*, p. 135.
Vittorio, N., and Juszkiewicz, R. 1987, *Ap. J.*, **314**, L29.
Zeldovich, Ya. B., 1972, *MNRAS*, **160**, 1P.